International Journal of Hydrogen Energy 95 (2024) 1151–1157

Contents lists available at ScienceDirect

International Journal of Hydrogen Energy

journal homepage: www.elsevier.com/locate/he

Exsolved perovskites for reliable SOFCs fed with dry biogas

Sebastian Vecino-Mantilla , Massimiliano Lo Faro *

Institute for Advanced Energy Technologies (ITAE) of the National Research Council of Italy (CNR), Via Salita S. Lucia sopra Contesse 5, 98126, Messina, Italy

ARTICLE INFO

Handling Editor: Ibrahim Dincer

Keywords:
Green deal
Perovskite
Electrochemistry
Gas-to-power
Renewable
REPowerEU

ABSTRACT

In-situ exsolution can be used to generate fine nanoparticles on the surface of certain perovskites with novel properties that make them attractive candidates for use as anodes or protective layers in solid oxide fuel cells (SOFCs) fed with conventional fuels such as biogas. This study describes the fabrication and characterization of two exsolved perovskites, nickel manganite (LSMN) and nickel cobaltite (LSCN). However, the main objective of this study was to conduct a comparative analysis of electrochemical studies employing such exsolved perovskites as a coating layer on two button cells derived from the same large area commercial SOFC. A comparison of diagnostic results before and after prolonged operation showed that LSCN exhibited better performance due to its higher catalytic activity that simplified fuel via a mechanism called as "shuttle mechanism". This behaviour was particularly evident in the EIS experiment, which, throughout the experiment fell on a simplified spectrum of only 2 semicircles and a reasonable total resistance of 0.316 Ω cm^2. Aside from performance that, in the case of LSCN, reached 0.68 W cm^{-2} @ 0.6V, such material appeared to be less affected by ohmic constraint due to its high reversibility. Nonetheless, as corroborated by the SEM reported in this paper, the superior advantage of using LSMN and LSCN as coatings in commercial SOFCs can be noticed in their ability to enhance the effectiveness of dry biogas-fed SOFCs by mitigating the formation of coke on the anode.

1. Introduction

In commercial Solid Oxide Fuel Cells (SOFCs) directly fueled by hydrocarbon compounds such as biogas, one of the main challenges is finding a way to counteract the risks arising from carbon formation and deposition during fuel conversion into power energy [1,2]. Consequently, the active phase on the anode side (*i.e.* Ni-YSZ, where YSZ stands for yttria stabilised zirconia) can be blocked, free spaces inside the anode can be obstructed, and the cell can break [3–5]. A cell with this issue performs poorly and is less durable. It may be possible to overcome these limitations by developing more reliable materials instead of Ni as the anode. Several studies report the existence of advanced anodes that are capable of competing with commercial anodes and appear more reliable than Ni for converting biofuels into electricity in SOFCs [6–9]. However, it would be necessary to understand, learn, and improve the entire production chain for cells and stacks in order to replace it with advanced materials. Clearly, this will require a revolution in cell manufacturing, stack assembly, and operational conditions, but it can also significantly impact the use of this technology in a positive way. This is the main reason why the producers of SOFC technology in the world have not yet suggested a real step change in materials used to construct SOFCs [10–14] that are substantially similar to those used in the first prototype of this technology demonstrated in the 1980s [15]. This technology advanced substantially in the last two decades with the development of anode-supported cells (ASC type), which allowed for a significant reduction in operating temperature [16–18]. Nevertheless, the current approach to tackling biofuel use problems still involves hardware to simplify fuel complexity (*e.g.* catalytic processors), but at a higher cost and complexity for the entire system [19–22]. Moreover, this approach also reduced performance (due to the dilution of fuel with water) and moderate risk of degradation from possible water management and chemical processor deficiencies [23–25].

By altering the anode's outer surface, organic fuels (e.g. syngas) may be efficiently converted and carbon formation due to metallic Ni could be mitigated. This strategy has recently been pursued by many scientists in this field, with a few different approaches reported in the literature [26,27]. One of these involves doping commercial anodes with alkali or noble metals to affect catalytic reactions, usually those involving fuel reforming [28–31]. In general, this approach requires sophisticated doping technology, which results in higher costs even though steam should still be added to the feed. In this way, the carbon deposition risk is effectively mitigated, even though the fuel must be obviously diluted,

* Corresponding author.
E-mail address: lofaro@itae.cnr.it (M. Lo Faro).

https://doi.org/10.1016/j.ijhydene.2024.04.326
Received 5 February 2024; Received in revised form 30 March 2024; Accepted 28 April 2024
Available online 9 May 2024

and some reoxidation risks for the anode and bipolar plate must be taken into account. The addition of an internal fuel processor could be a viable approach in other cases since fuel conversion can be controlled precisely [32–36]. In this approach, water should also be provided to the inlet, while the stack assembly should have sufficient space to accommodate the internal reformer, while temperature control is another critical issue. These achievements led to the development of a novel approach based on the modification of the surface of commercial cells using advanced materials. To be effective, these materials must be cheaper than noble metals, have resistant properties to carbon deposition, and must be applied with practical procedures similar to those used for making commercial cells. As well, they should possess promising properties for catalytic and electrocatalytic conversion of organic fuels to enhance the kinetics of the mechanisms involved, especially those requiring low steam content or dry conditions.

Hence, an additional anodic active layer in commercial SOFCs based on exsolved perovskites was successfully demonstrated to overcome these shortcomings [37,38]. Using such materials as a functional layer for the anode of commercial cells (i.e. Ni-YSZ) enables the cell to benefit from optimum thermal and chemical conditions for internal reforming of organic fuels. As fuels are electrochemically oxidized, water and CO_2 are formed on the anode, which reacts with the inlet gas once it crosses the protective layer. This results in the production of syngas as well as creating a closed chemical loop that promotes fuel simplification, also known as the "shuttle mechanism" [39,40]. In addition, an active layer protects a commercial cell from direct contact with organic fuels, which can crack under a wide range of conditions on the Ni-YSZ anode [41]. These conditions can result from the peculiar features of an exsolved perovskite that is generally characterized by a highly stable surface and electrocatalytically active nanoparticles uniformly distributed on the surface with a high carbon coking tolerance in a hydrocarbon fuel atmosphere [40,42–48].

To accomplish this, two catalytic materials used as a coating layer for direct dry biogas-fed SOFCs were electrocatalytically analyzed and compared in this paper. The materials compared in this paper are manganite- and cobaltite-based perovskites that were exsolved by adding Ni and thermally treated in two steps under oxidizing and reducing atmospheres. These materials clearly refer to two of the most commonly used cathodes used in this technology. The manganite based perovskite was quite exclusively used for the traditional SOFC technology operating at temperatures beyond 800 °C using a single electrolyte based on YSZ [49,50]. Instead, most advanced cells use perovskites made of cobalt, despite the fact that the cost of this metal is rising so rapidly that EU regulations include it on their critical raw material list [51]. A comparison of these two perovskites opportunely doped with Ni to improve their anodic performances is presented in this paper to determine whether they can have major potential for use as a fine protective coating on conventional SOFC anodes. The resulting stoichiometries examined were $La_{1.5}Sr_{1.5}Mn_{1.5}Ni_{0.5}O_{7\pm\delta}$ (referred to as LSMN) and $La_{1.5}Sr_{1.5}Co_{1.5}Ni_{0.5}O_{7\pm\delta}$ (referred to as LSCN) both showing a Ruddlesden-Popper (RP) phase. In order to enhance oxygen spillover characteristics, as well as electron and ion percolation, these materials were mixed with gadolinium-doped ceria (GDC) prior to their use as a coating layer.

2. Materials and methods

The citrate complexation method, also known as Pechini synthesis was used to synthesize the materials [52–54]. To conduct such preparations, stoichiometric amounts of high-purity $La(NO_3)_3.6H_2O$ (≥99.9% Alfa), $Sr(NO_3)_2$ (≥99% Aldrich) were used for the A-site of the RP phase, while $Ni(NO_3)_2.6H_2O$ (≥99.999 % Aldrich), and $Mn(NO_3)_2.6H_2O$ (≥99.99% Aldrich) or $Co(NO_3)_2.6H_2O$ (≥99.99 % Aldrich) for the B-site in the LSMN and LSCN specimens, respectively. Initially, the precursors were dissolved in citric acid (≥99.5% Sigma-Aldrich) aqueous solution at a molar ratio of CA:(metal ion) = 3:1. Under constant stirring, the solution was gradually heated from room temperature to 120 °C. In this synthesis, ethylene glycol (≥99%, Aldrich) was used as a polymerizing agent. Subsequently, all organic materials were removed from the gel by drying it at 300 °C for 2 h and 500 °C for 3 h. After grinding the specimens, the resulting powders were pelletized and sintered for 12 h at 1300 °C to obtain satisfactory crystallization.

As-calcined pellets of LSMN and LSCN were again pulverised and ground in a planetary ball mill at 250 RPM for 6 h with commercial gadolinium-doped ceria (GDC), specifically $Ce_{0.9}Gd_{0.1}O_2$. The high oxygen storage capacity of GDC 10% combined with its acceptable electrical conductivity makes it suitable for electrode manufacturing [55–57]. Afterwards, LSCN + GDC and LSMN + GDC were mixed with organic additives (8 wt% terpineol, 2 wt% polyvinyl butyral resin (BUTVAR B-98) and 2-propanol) in a planetary ball mill for 2 h to obtain inks to be deposited as a coating layer on commercial cells [45].

A single large-area (10 cm × 10 cm) commercial anode-supported solid oxide fuel cell (ASC), manufactured by InDEC® was used for electrocatalytic tests. This cell was laser cut into button cells, each one with a 2 cm^2 active area. The cells were composed of NiO-YSZ/YSZ/LSM, where YSZ stands for $(ZrO_2)_{0.92}(Y_2O_3)_{0.08}$, while LSM stands for $La_{0.8}Sr_{0.2}MnO_3$. Temperatures above 800 °C were optimal for these types of cells. After applying gold paste to both electrodes, the cells were annealed at 500 °C for 10 min to ensure ideal contact with the external electrochemical equipment.

A painting procedure was used to apply LSMN + GDC and LSCN + GDC inks on the anode of commercial cells, followed by the post-annealing step a 500 °C. The result of this procedure was a protective layer of approximately 20 mg cm^{-2} of LSMN + GDC and LSCN + GDC.

The next step was to conduct electrochemical testing on the button cells. One by one, the cells containing LSMN + GDC and LSCN + GDC were sealed with ceramic paste (AREMCO 316) at the end of an alumina tubular reactor, with the anode facing the inner of the tube and the cathode facing static air. Gold wires welded to each electrode ensured the electrical connection to measure both current and voltage. After this, the reactor mounting the cell was placed in a tubular furnace for prolonged testing at high temperatures (see Fig. 1). Curing the sealing paste according to the AREMCO procedure was a preliminary procedure. The standard procedure was to place the cell in diluted H_2 (20% in He) for 12 h at 800 °C to achieve the complete reduction of the Ni-anode before testing. The initial operation was conducted with diluted H_2 (60% in He) as a baseline, followed by dry simulated biogas (*i.e.* CH_4:CO_2 = 60 vol %:40 vol%) at a flow rate of 15 cm^3 min^{-1}. As part of electrochemical studies, open circuit voltages (OCV), polarization curves (current-potential curves, I–V curves), impedance spectroscopy (EIS), and long-duration galvanostatic measurements were performed using a Bio-Logic diagnostic tool equipped with a booster of 100 A and a frequency response analyser for impedance spectroscopy.

For the physicochemical analysis, a Bruker D8 ADVANCE diffractometer operating at 40 kV and 40 mA was used to determine the crystallinity of specimens applied as coating layers. XRD patterns were analyzed using Bruker's Evaluation Software for Crystallography (EVA) and phases were assigned according to the Crystallography Open Database (COD). A scanning electron microscope (SEM) FEI XL 30 was used to study spent cells' morphology.

3. Results and discussions

A first study determined the phase structure of exsolved perovskites used as functional layers for commercial SOFC cells. Fig. 2a and b shows the XRD patterns of samples calcined at 1300 °C and reduced at 800 °C. There is evidence for high phase purity for the LSMN in the XRD related to calcined specimens (Fig. 2a), and it was previously identified as a Ruddlesden-Popper (RP) phase with n = 2, containing two perovskite units between rock-salt layers based on $La_{1-x}Sr_xO$, and with stoichiometry $La_{1.5}Sr_{1.5}Mn_{1.5}Ni_{0.5}O_{7\pm\delta}$ [52]. As opposed to LSMN, LSCN did not appear to be a pure phase according to the XRD results. Specifically, two

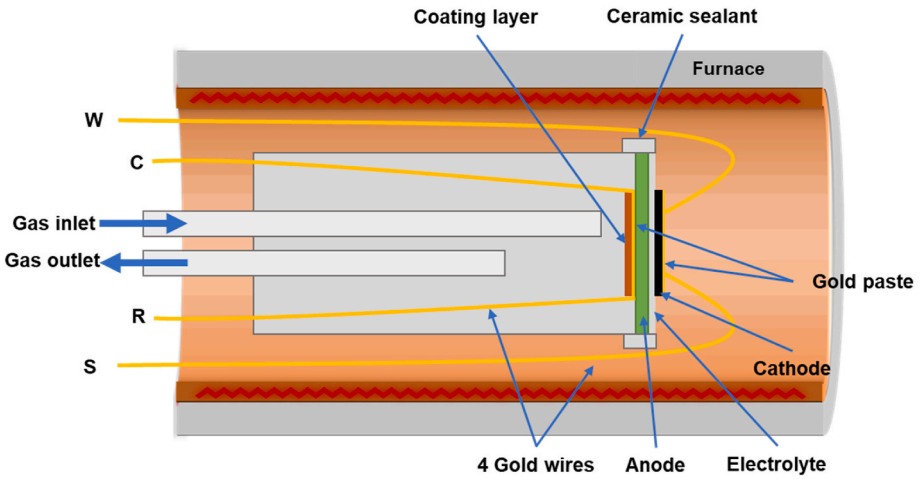

Fig. 1. A schematic of the experimental setup for testing cells.

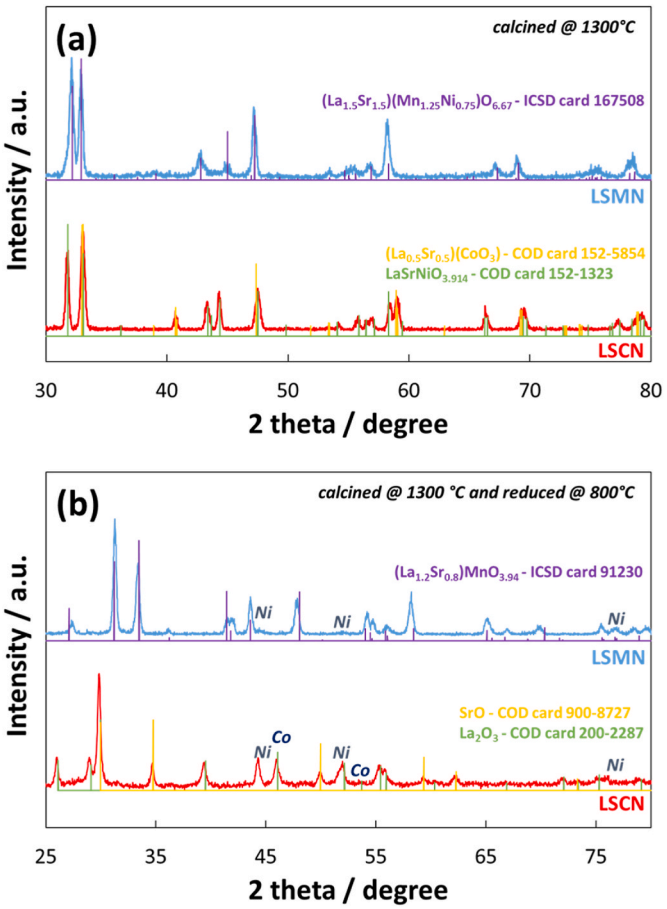

Fig. 2. XRD patterns of LSMN and LSCN samples after calcination at 1300 °C (a) and subsequent reduction at 800 °C (b).

structures were observed, which led to Co-based perovskites (*i.e.* $La_{0.5}Sr_{0.5}CoO_3$, COD card 152–5854 [58]) and Ni-based RP-phase (*i.e.* $La_{0.5}Sr_{0.5}NiO_4$, COD card 152–1323 [59]). As far as the scope of this paper is concerned, we will refer to it as LSCN even though it is not a pure phase. Upon exposure to a reducing atmosphere and high temperatures (>750 °C), Ni within the crystalline phase exsolves as embedded nanoparticles possessing an oxide composition, as illustrated in Fig. 2b, where the LSMN assumed the feature of $La_xSr_{1-x}MnO_{4\pm\delta}$ stoichiometry (LSM, RP n = 1) without any other impurities [52,60]. A similar phenomenon was observed for the LSCN, where metallic Ni and Co were partially depleted and exsolved to the surface, increasing the complexity of the initial perovskite. According to our recent paper [39], LSCN has however demonstrated a reversible mechanism, which accomplishes the mechanism occurring under anodic conditions. In light of this reversible behaviour, LSCN may be a promising material for electrochemical devices, although further research is necessary to determine its full potential.

For the purpose of examining the electrochemical behaviour of cells coated with functional layers (LSCN + GDC or LSMN + GDC), we conducted durability tests lasting approximately 270 h in each case following the standard procedures discussed in the experimental section

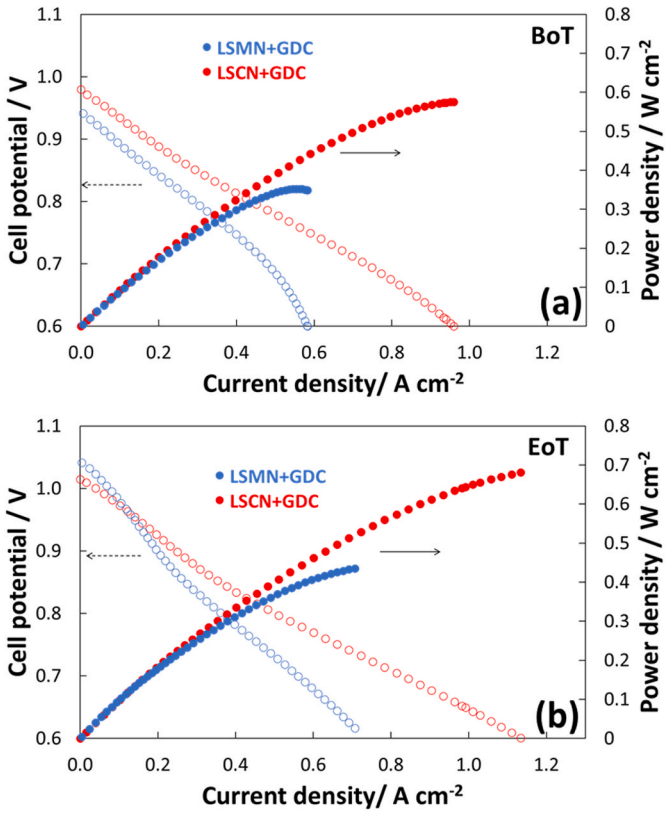

Fig. 3. Polarization and power density curves of the cells coated with LSMN + GDC and LSCN + GDC using biogas at 800 °C. At the beginning of the test (a) and at the end of the test, after 270 h of operation (b).

(not shown here). Upon reducing the anode (*i.e.* Ni-YSZ), dry biogas was fed to assess how the coatings enhanced cells' behaviour. Fig. 3a and b compare the power density and polarization curves measured in dry biogas at 800 °C at the beginning (BoT) and end (EoT) of the durability test. At the beginning of the tests, the OCVs recorded in both experiments were lower than 1 V, with the LSMN-coated cell showing a higher ohmic constraint than the LSCN-coated cell (Fig. 3a). Based on these initial experimental results, the LSMN-coated cell produced a maximum power density of 0.35 W cm^{-2} @0.6V, while the LSCN-coated cell reached a maximum power density of 0.57 W cm^{-2} @0.6V. However, over the course of the experiment, there was a gradual increase in OCV, which at the end exceeded 1 V for both cells investigated (Fig. 3b). LSMN-coated cells showed the highest OCV, though their performance remained limited by ohmic constraints also at the end of the durability test (Fig. 3b). Despite this, both cells showed enhanced performance with time, reaching maximum power densities of 0.44 W cm^{-2} @0.6V for LSMN-coated cell and 0.68 W cm^{-2} @0.6V for LSCN-coated cell. A significant part of these enhancements can be attributed to increased potential, as shown in Fig. 3b.

This increase in OCV can be explained by what might be happening in the anode cell during the operation. A conceivable explanation of this observation could be provided by one of our previous papers presenting a "shuttle mechanism" for ferrite-based exsolved perovskites coated on commercial cells. This mechanism relies on a combination of chemical and electrochemical reactions occurring at the coating layer, allowing the oxidation of biogas with the help of H_2O and CO_2 produced during fuel oxidation and reducing the risk of methane cracking. Several reactions can occur in the anode compartment. Since biogas contains a high percentage of CO_2, dry reforming of methane is quite feasible at first:

$$CH_4 + CO_2 \rightleftarrows 2CO + 2H_2 \quad \text{(reaction 1)}$$

As a result of this reaction, CO and H_2, which have better mobility than biogas, can diffuse at the anode-electrolyte interface and be oxidized to form H_2O and CO_2 and obviously power energy:

$$H_2 + O^{2-} \rightarrow H_2O + 2\,e^- \quad \text{(reaction 2)}$$

$$CO + O^{2-} \rightarrow CO_2 + 2\,e^- \quad \text{(reaction 3)}$$

It is possible for H_2O and CO_2 to diffuse to the outer side of the cell where the partial pressure of methane is sufficiently high and take part in steam reforming:

$$CH_4 + H_2O \rightarrow CO + 3H_2 \quad \text{(reaction 4)}$$

As a result, the OCV was determined by the complex gas mixture in the anode compartment, which changed over time, reflecting also the catalytic properties of the coating layers.

As a means of illustrating the overall impact of cell constraints on their performances, Fig. 4a and b shows the first derivative curves of the related polarization curves (Fig. 3a and b). According to Fig. 4a, at the beginning of the experiment, the LSMN-coated cells had a significantly higher Area Specific Resistance (ASR) than the LSCN-coated cells. In addition to a significantly higher activation constraint (curves at low current densities) indicating a lower kinetic towards the oxidation of biogas, the region mainly affected by the ohmic constraint (intermediate current densities) was not optimal compared to the LSCN-coated cell. A rapid increase in resistance was observed starting at 0.2 A cm^{-2}, which indicated a dramatic loss of conductivity. The reason for this effect is that the LSMN was derived from the LSM electrocatalyst, one of the oldest cathode electrocatalysts used in SOFCs, while the LSCN was derived from the LSC electrocatalyst, one of the most widely used electrocatalysts in advanced SOFCs today because of its much lower overpotentials [61]. Fig. 4b illustrates how the LSMN's features changed at the end of the test, while the LSCN's remained mostly unchanged. LSMN-coated cells showed a relatively high activation control, which is

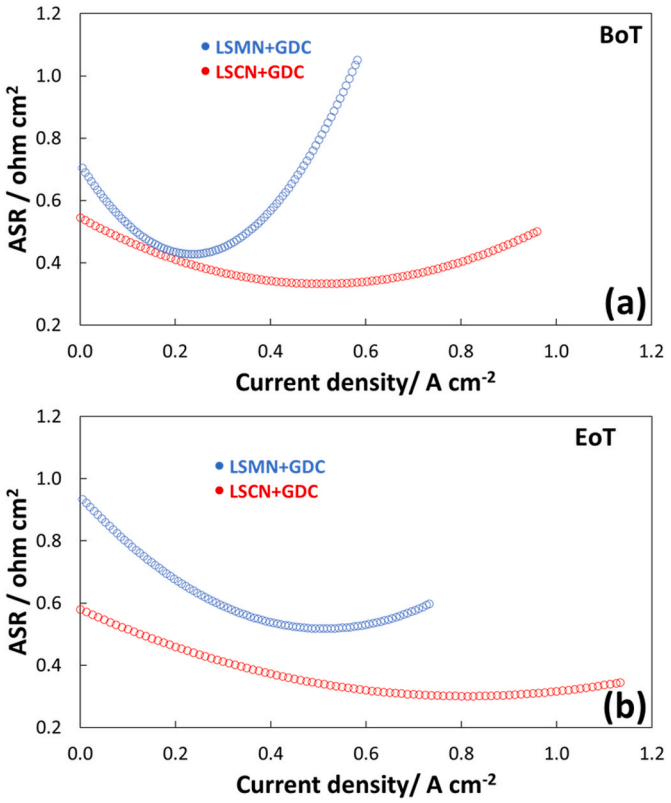

Fig. 4. The first derivative curves obtained for the cells coated with LSMN + GDC and LSCN + GDC at the beginning of the experiment (a) and after 270 h (b) of operation.

consistent with an electrocatalyst with moderate properties for catalytic reactions involving methane, although its ohmic constraint became relatively low. Regarding the diffusion constraint, generally occurring at high current densities, only the cell coated with the LSCN showed moderate control, which is explained by the fact that the characteristic I–V curves were collected up to 0.6 V amply before the power density curve reached its maximum (Fig. 3a and b).

Further diagnosis was conducted by measuring impedance spectra at 0.8 V and 0.7 V in the presence of dry biogas during cell operation (Fig. 5a–d). Initially, the spectra showed three well-defined semicircles associated with the main mechanisms involved during the conversion of fuel into energy. This is particularly evident in the case of LSMN-coated cell, which, as discussed above, had limited catalytic activity (Fig. 5a and c). Thus, it is likely that one semicircle is caused by oxygen reduction at the cathode, while the other two could be caused by the oxidation of complex fuel at the anode [62,63]. The oxidation of H_2 and CO can occur rapidly and may generate the semicircle at higher frequencies [64], while the direct oxidation of methane may be responsible for the semicircle at lower frequencies [65]. While this event is probable, kinetically it is not preferred since it involves the exchange of eight electrons in a single reaction. According to the first derivative curves in Fig. 4b, such behaviour still prevailed in the EIS of LSMN-coated cell even at the end of the test (Fig. 5b and d). A simplified EIS profile conforming to just two semicircles was observed in the LSCN-coated cell collected after the testing. This indicates that the biogas was mostly converted into syngas and the conversion into energy power was primarily accomplished by oxidizing H_2 and CO. An event such as this would be possible only if a catalyst *(i.e.* LSCN) could catalyze efficiently the conversion of biogas into syngas.

At high frequencies, the intercept of the EIS with the x-axis is known as the series resistance (Rs) and it is often associated with the electrolyte conductivity of an ideal SOFC cell [66]. Nevertheless, such resistance

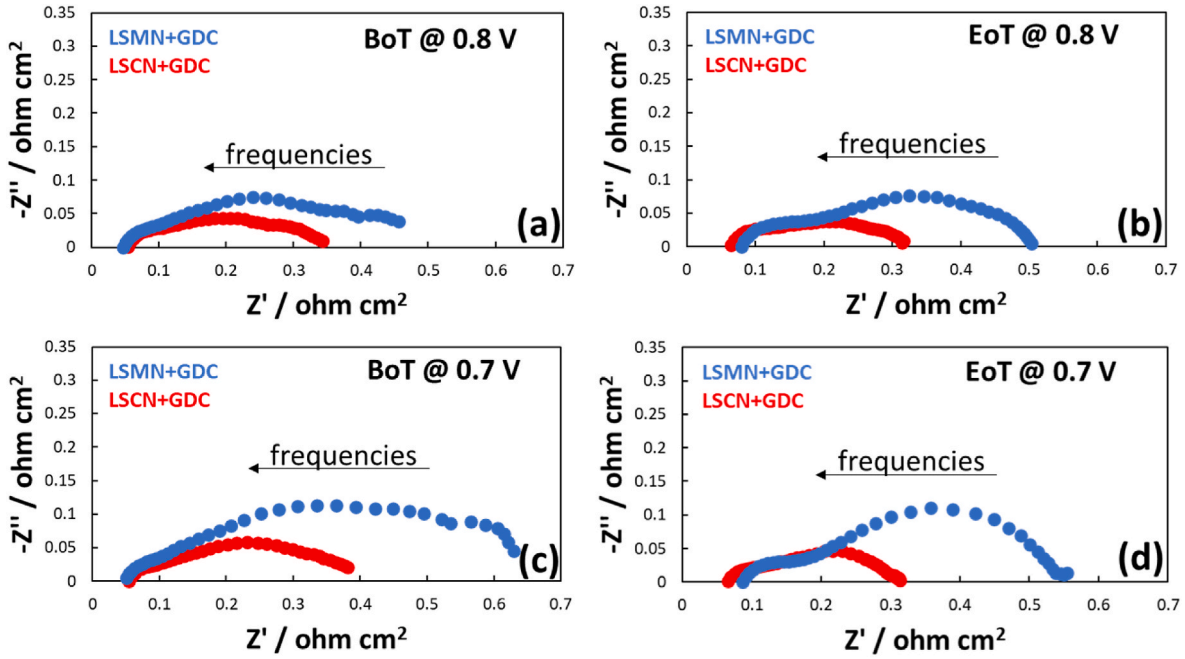

Fig. 5. Comparison of impedance spectra collected before and after the durability test (BoT and EoT).

can increase with the aging of practical cells due to coarsening of Ni in the anode, reducing electronic percolation. Moreover, an additional layer based on materials that are not optimized for ionic-electronic conductivity, such as those used in these experiments, can also contribute to the increase of resistance over time. As it pertains to these experiments, we noticed that the Rs increased during the durability test. Based on Fig. 5a and b, the LSMN-coated cell exhibited the strongest effect, with an initial Rs @ 0.8 V of 0.045 Ω cm^2 reaching 0.079 Ω cm^2 at EoT. Rs @ 0.7 V exhibited similar behaviour, with values moving from 0.047 Ω cm^2 at BoT to 0.087 Ω cm^2 at EoT (Fig. 5c and d). The results of these experiments also revealed that Rs was affected by the potential at which EIS is acquired; the effect was particularly apparent for LSMN-coated cells. There was such an effect at the BoT, but it was particularly evident at the EoT, where the Rs value was 0.079 Ω cm^2 @ 0.8 V, increasing to 0.087 Ω cm^2 @ 0.7 V (Fig. 5b and d). The change in slope of the ASR curves shown in Fig. 4a–b between 0.8 V (*i.e.* 0.36 A cm^{-2}) and 0.7 V (*i.e.* 0.56 A cm^{-2}) may explain this effect. It is likely that the occurrence of such a phenomenon was influenced by a superficial modification of LSMN, which in turn changed its conductivity.

Table 1 summarizes Rs and Rt (defined as total resistance derived from the intercept of EIS at low frequencies with the x-axis) for all experiments. By comparing these data, it is apparent that the Rt decreased over the course of the durability test and this is what led to the increased performances observed in Fig. 3a and b. Only the Rt at 0.8 V measured for the LSMN-coated cell deviates moderately from this trend, due to an ASR more dependent upon the activation constraint as observed in Fig. 4b.

Table 1
Rs and Rt values at the beginning and end of the durability test.

	Coating layer	Rs @ BoT [Ω·cm^2]	Rt @ BoT [Ω·cm^2]	Rs @ EoT [Ω·cm^2]	Rt @ EoT [Ω·cm^2]
0.8 V	LSMN + GDC	0.045	0.456	0.079	0.503
	LSCN + GDC	0.051	0.342	0.061	0.316
0.7 V	LSMN + GDC	0.047	0.629	0.087	0.555
	LSCN + GDC	0.052	0.381	0.062	0.313

The microstructure of the supporting anode based on Ni-YSZ and coating layers after 270 h at 800 °C is shown in Fig. 6. There was no significant Ni coarsening in each cell studied, and the electrode (Ni-YSZ) microstructure appeared uniform with high porosity for adequate mass diffusion of reactants and products (Fig. 6a and c). It is noteworthy that anode pores appear without carbon deposits, which contributes to the remarkable cell performance observed in the I–V curves (Fig. 3a and b). This state is caused by the synergistic effect generated by the presence of H_2O and ionic oxygen concurrently in the anode, which suppresses parasitic reactions, as well as by the presence of the coating layer, which simplified fuel, reduced coking, and prevented cell deactivation. According to Fig. 6b and d, the coating layers contained fine-embedded nanoparticles with spherical (LSMN) and cauliflower (LSCN) shapes. The uniform distribution of fine particles and their strong interaction with the support, prevent any possibility of coarsening, thereby preventing any possible loss of active surface area. Additionally, the exsolved LSCN particles have a much higher surface area than smooth spherical particles in LSMN, allowing them to perform better as a coating layer, as demonstrated by the electrochemical tests. As for the Ni-YSZ anode, there is no evidence of any carbonaceous species on the porosity of the coating layers, indicating the effectiveness and robustness of these experiments.

4. Conclusions

A pair of button cells derived from the same anode-supporting commercial cell, were coated with two electrocatalysts developed for operating in dry biogas and studied to demonstrate the feasibility of using exsolved perovskites to mitigate the risks associated with using such dry fuel in commercial cells. A study was conducted to compare the behaviours and characteristics of commercial cells before and after prolonged use in order to gain insight into the potential benefits of this approach. According to this comparison, the exsolved LSCN layer performed better since the B-site of this perovskite contains Co instead of Mn as for LSMN (the other exsolved perovskite studied in this paper). These results were attributed to enhanced O^{2-} transport into crystal structures as well as better electronic mobility, which improved kinetics and conductivity. Particularly, such behavior was evident in the comparison of the first derivative of the polarization curves. The LSCN had a

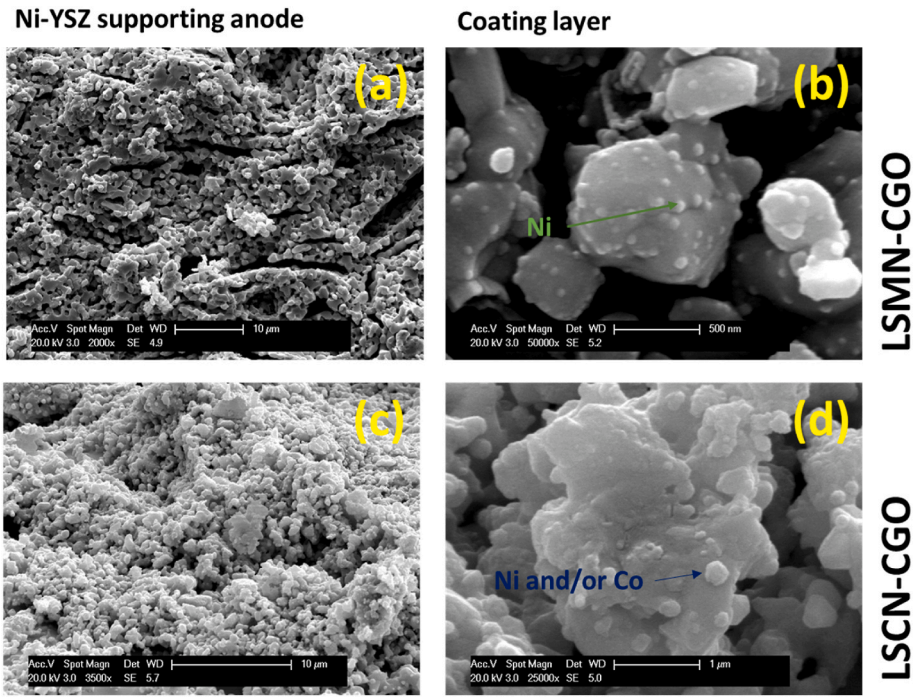

Fig. 6. SEM images of post-reaction cells coated with LSMN-GDC and LSCN-GDC.

lower ASR in the intermediate current range, which contributed to the better slope of the polarization curves, allowing for superior performance at 0.6 V (i.e. 0.35 W cm^{-2} for the cell coated with LSMN and 0.57 W cm^{-2} for the cell coated with LSCN). In consequence of prolonged operation, enhanced performances (i.e. 0.44 W cm^{-2} for the cell coated with LSMN and 0.681 W cm^{-2} for the cell coated with LSCN) were achieved due to a number of factors, including an increased open circuit voltage (i.e. 1.04 V for the cell coated with LSMN and 1.01 V for the cell coated with LSCN), as well as an increase in reagent diffusivity as indicated by EIS analyses which showed a simplified spectrum and by the first derivative curves that showed lower ASR at 0.6 V (i.e. approx. 0.6 Ω cm^2 for the cell coated with LSMN and 0.34 Ω cm^2 for the cell coated with LSCN. According to electrochemical analyses, both of these changes are the result of shuttle mechanisms initiated by exsolved perovskites, albeit with some differences. Furthermore, SEM analysis showed that, although both LSCN and LSMN have surfaces characterized by fine particles, LSCN likely has a higher surface active area due to the cauliflower features exhibited by the embedded particles. As a result of these different characteristics, the LSCN showed a more pronounced tendency to promote the "shuttle mechanism". As a result of producing syngas, the electrochemical reactions occurring at the anode and producing electricity were simplified, as they involve primarily H_2 and CO, which in optimized SOFCs operating at 800 °C have similar kinetics. EIS clearly demonstrated this difference in behavior between the two cells investigated. After the reaction, both cells showed no carbonous species, indicating that this type of approach may reduce the risks associated with using hydrocarbon fuel directly in commercial SOFCs.

In light of these results and literature data concerning the redox properties of both LSCN and LSMN, it seems that LSCN might be particularly suitable as an anode or coating layer in SOFCs, although there is space for further improvement in reducing temperatures and improving electrical conductivity within the coating layer.

CRediT authorship contribution statement

Sebastian Vecino-Mantilla: Data curation, Formal analysis, Investigation, Visualization, Writing – original draft. **Massimiliano Lo Faro:** Conceptualization, Data curation, Funding acquisition, Methodology, Project administration, Resources, Supervision, Validation, Writing – original draft, Writing – review & editing.

Declaration of competing interest

The authors declare that they have no known competing financial interests or personal relationships that could have appeared to influence the work reported in this paper.

Acknowledgements

This research was funded by the European Union – NextGeneration EU from the Italian Ministry of Environment and Energy Security POR H_2 AdP MMES/ENEA with involvement of CNR and RSE, PNRR - Mission 2, Component 2, Investment 3.5 "Ricerca e sviluppo sull'idrogeno", CUP: B93C22000630006. In addition, the authors acknowledge the MUR for funding the PRIN project SUPERH2, CUP E53D23009400006 and PRIN PNRR project OxCellenT, CUP B53D23027440001. Dr Lo Faro acknowledges the ITELECTROLAB CUP B43C22000870001, the Joint lab between CNR-ITAE and IQSC-USP financed by the National Research Council of Italy (CNR) and the bilateral project "FlexPower- Solid Oxide Fuel Cell fed with Biofuel as an Electric Flexible Provider in a Distributed Grid" CUP B45F22000030001 granted by MAECI.

References

[1] Marina OA, Mogensen M. High-temperature conversion of methane on a composite gadolinia-doped ceria–gold electrode. Appl Catal Gen 1999;189:117–26.
[2] Park S, Vohs JM, Gorte RJ. Direct oxidation of hydrocarbons in a solid-oxide fuel cell. Nature 2000;404:265–7.
[3] Irvine JTS, Sauvet A. Improved oxidation of hydrocarbons with new electrodes in high temperature fuel cells. Fuel Cell 2001;1:205–10.
[4] Sin A, Kopnin E, Dubitsky Y, Zaopo A, Aricò AS, La Rosa D, et al. Performance and life-time behaviour of NiCu–CGO anodes for the direct electro-oxidation of methane in IT-SOFCs. J Power Sources 2007;164:300–5.
[5] Li J, Croiset E, Ricardez-Sandoval L. Theoretical investigation of the methane cracking reaction pathways on Ni (1 1 1) surface. Chem Phys Lett 2015;639:205–10.
[6] Gorte RJ, Park S, Vohs JM, Wang C. Anodes for direct oxidation of dry hydrocarbons in a solid-oxide fuel cell. Adv Mater 2000;12:1465–9.
[7] Atkinson A, Barnett S, Gorte RJ, Irvine JTS, McEvoy AJ, Mogensen M, et al. Advanced anodes for high-temperature fuel cells. Nat Mater 2004;3:17–27.

[8] Cowin PI, Petit CTG, Lan R, Irvine JTS, Tao S. Recent progress in the development of anode materials for solid oxide fuel cells. Adv Energy Mater 2011;1:314–32.
[9] Xu Q, Guo Z, Xia L, He Q, Li Z, Temitope Bello I, et al. A comprehensive review of solid oxide fuel cells operating on various promising alternative fuels. Energy Convers Manag 2022;253:115175.
[10] Bertoldi M, Bucheli O, Ravagni AV. Development, manufacturing and deployment of SOFC-based products at SOLIDpower. ECS Trans 2017;1:117–23. ed.
[11] Arkenberg GB, Swartz SL, Sellers CT. Update on Nexceris' SOFC stack technology. ECS Trans 2017;1:1805–14. ed.
[12] Aguilo-Rullan A, Atanasiu M, Biebuyck B, Lymperopoulos N, Marenco C, Tsimis D. The status of SOFC and SOEC R&D in the European fuel cell and hydrogen joint undertaking programme. ECS Trans 2017;1:41–61. ed.
[13] Hickey D, Alinger M, Shapiro A, Brown K, Striker T, Wang H, et al. Stack development at GE-fuel cells. ECS Trans 2017;1:107–16. ed.
[14] Mai A, Fleischhauer F, Denzler R, Schuler A. Progress in HEXIS' development: galileo 1000 N and HEXIS' next generation SOFC system. ECS Trans 2017;1:97–106. ed.
[15] Singhal SC. Advances in solid oxide fuel cell technology. Solid State Ionics 2000;135:305–13.
[16] Murata K, Shimotsu M. Fabrication and evaluation of electrode-supported planar SOFC. Denki Kagaku 1997;65:38–43.
[17] Dokiya M. SOFC system and technology. Solid State Ionics 2002;152–153:383–92.
[18] Holtappels P, Stimming U. Solid oxide fuel cells (SOFC). John Wiley & Sons, Ltd; 2010.
[19] Bove R, Sammes NM. Thermodynmic analysis of SOFC systems using different fuel processors. Fuel Cell Science, Engineering and Technology - 2004 2004:461–6.
[20] Piroonlerkgul P, Assabumrungrat S, Laosiripojana N, Adesina AA. Selection of appropriate fuel processor for biogas-fuelled SOFC system. Chem Eng J 2008;140:341–51.
[21] Yoon S, Lee S, Bae J. Development of a self-sustaining kWe-class integrated diesel fuel processing system for solid oxide fuel cells. Int J Hydrogen Energy 2011;36:10302–10.
[22] Braun RJ, Vincent TL, Zhu H, Kee RJ. Chapter 7 - analysis, optimization, and control of solid-oxide fuel cell systems. In: Sundmacher K, editor. Advances in chemical engineering. Academic Press; 2012. p. 383–446.
[23] Cimenti M, Hill JM. Thermodynamic analysis of solid oxide fuel cells operated with methanol and ethanol under direct utilization, steam reforming, dry reforming or partial oxidation conditions. J Power Sources 2009;186:377–84.
[24] Greco A, Sorce A, Littwin R, Costamagna P, Magistri L. Reformer faults in SOFC systems: experimental and modeling analysis, and simulated fault maps. Int J Hydrogen Energy 2014;39:21700–13.
[25] Chatrattanawet N, Saebea D, Authayanun S, Arpornwichanop A, Patcharavorachot Y. Performance and environmental study of a biogas-fuelled solid oxide fuel cell with different reforming approaches. Inside Energy 2018;146:131–40.
[26] Dokmaingam P, Irvine JTS, Assabumrungrat S, Charojrochkul S, Laosiripojana N. Modeling of IT-SOFC with indirect internal reforming operation fueled by methane: effect of oxygen adding as autothermal reforming. Int J Hydrogen Energy 2010;35:13271–9.
[27] Aguiar P, Chadwick D, Kershenbaum L. Modelling of an indirect internal reforming solid oxide fuel cell. Chem Eng Sci 2002;57:1665–77.
[28] Liu L, Yang Q, Yang W, Qi X, Sun C, Chen L. Li/Na modified Ni-SDC anode for methane-fueled solid oxide fuel cells. ECS Trans 2015;68:1403.
[29] Hibino T, Hashimoto A, Yano M, Suzuki M, Sano M. Ru-catalyzed anode materials for direct hydrocarbon SOFCs. Electrochim Acta 2003;48:2531–7.
[30] Nabae Y, Yamanaka I. Alloying effects of Pd and Ni on the catalysis of the oxidation of dry CH4 in solid oxide fuel cells. Appl Catal Gen 2009;369:119–24.
[31] Babaei A, Jiang SP, Li J. Electrocatalytic promotion of palladium nanoparticles on hydrogen oxidation on Ni/GDC anodes of SOFCs via spillover. J Electrochem Soc 2009;156:B1022.
[32] Park YM, Kim H. An additional layer in an anode support for internal reforming of methane for solid oxide fuel cells. Int J Hydrogen Energy 2014;29:16513–23. ed.
[33] Lin Y, Zhan Z, Barnett SA. Improving the stability of direct-methane solid oxide fuel cells using anode barrier layers. J Power Sources 2006;158:1313–6.
[34] Zhan Z, Barnett SA. An octane-fueled solid oxide fuel cell. Science 2005;308:844–7.
[35] Zhang P, Yang Z, Jin Y, Liu C, Lei Z, Chen F, et al. Progress report on the catalyst layers for hydrocarbon-fueled SOFCs. Int J Hydrogen Energy 2021;46:39369–86.
[36] Santoro M, Di Bartolomeo E, Luisetto I, Aricò AS, Squadrito G, Zignani SC, et al. Insights on the electrochemical performance of indirect internal reforming of biogas into a solid oxide fuel cell. Electrochim Acta 2022;409.
[37] Lo Faro M, Reis RM, Saglietti GGA, Sato AG, Ticianelli EA, Zignani SC, et al. Nickel-Copper/Gadolinium-doped Ceria (CGO) composite electrocatalyst as a protective layer for a Solid-Oxide Fuel Cell anode fed with ethanol. Chemelectrochem 2014;1:1395–402.
[38] Lo Faro M, La Rosa D, Nicotera I, Antonucci V, Aricò AS. Electrochemical behaviour of propane-fed solid oxide fuel cells based on low Ni content anode catalysts. Electrochim Acta 2009;54:5280–5.
[39] Lo Faro M, Ometto FB, Zignani SC, Vecino-Mantilla S, Perez J, Ticianelli E. Exploring the use of bioethanol for high-temperature electrolysis of water. Electrochim Acta 2023;466.
[40] Lo Faro M, Campagna Zignani S, Arico AS. Lanthanum ferrites-based exsolved perovskites as fuel-flexible anode for solid oxide fuel cells. Materials 2020;13:3231.
[41] Lo Faro M, Zignani SC, Trocino S, Antonucci V, Aricò AS. New insights on the co-electrolysis of CO_2 and H_2O through a solid oxide electrolyser operating at intermediate temperatures. Electrochim Acta 2019;296:458–64.
[42] Yu Yao YF. The oxidation of hydrocarbons and CO over metal oxides. IV. Perovskite-type oxides. J Catal 1975;36:266–75.
[43] Shimizu T. Partial oxidation of hydrocarbons and oxygenated compounds on perovskite oxides. Catal Rev 1992;34:355–71.
[44] Gunasekaran N, Rajadurai S, Carberry JJ, Bakshi N, Alcock CB. Surface characterization and catalytic properties of $La_{1-x}A_xMO_3$ perovskite type oxides. Part I. Studies on $La_{0.95}Ba_{0.05}MO_3$ (M = Mn, Fe or Co) oxides. Solid State Ionics 1994;73:289–95.
[45] Lo Faro M, Arico AS. Electrochemical behaviour of an all-perovskite-based intermediate temperature solid oxide fuel cell. Int J Hydrogen Energy 2013;38:14773–8.
[46] Yang G, Zhou W, Liu M, Shao Z. Enhancing electrode performance by exsolved nanoparticles: a superior cobalt-free perovskite electrocatalyst for solid oxide fuel cells. ACS Appl Mater Interfaces 2016;8:35308–14.
[47] Hou N, Yao T, Li P, Yao X, Gan T, Fan L, et al. A-site ordered double perovskite with in situ exsolved core-shell nanoparticles as anode for solid oxide fuel cells. ACS Appl Mater Interfaces 2019;11:6995–7005.
[48] Sun Z, Fan W, Bai Y. A flexible method to fabricate exsolution-based nanoparticle-decorated materials in seconds 2022;9:2200250.
[49] Ippommatsu M, Sasaki H, Otoshi S. Evaluation of the cost performance of the SOFC cell in the market. Int J Hydrogen Energy 1996;21:129–35.
[50] Huijsmans JPP, Van Berkel FPF, Christie GM. Intermediate temperature SOFC - a promise for the 21st century. J Power Sources 1998;71:107–10.
[51] Blengini G, Latunussa C, Eynard U, Matos C, Georgitzikis K, Pavel C, et al. Study on the EU's list of critical raw materials. 2020. Final Report2020.
[52] Vecino-Mantilla S, Gauthier-Maradei P, Huvé M, Serra JM, Roussel P, Gauthier GH. Nickel exsolution-driven phase transformation from an n=2 to an n=1 ruddlesden-popper manganite for methane steam reforming reaction in SOFC conditions. ChemCatChem 2019;11:4631–41.
[53] Vecino-Mantilla S, Quintero E, Fonseca C, Gauthier GH, Gauthier-Maradei P. Catalytic steam reforming of natural gas over a new Ni exsolved ruddlesden-popper manganite in SOFC anode conditions, vol. 12; 2020. p. 1453–66.
[54] Vecino-Mantilla S, Simon P, Huvé M, Gauthier G, Gauthier-Maradei P. Methane steam reforming in water-deficient conditions on a new Ni-exsolved Ruddlesden-Popper manganite: coke formation and H2S poisoning. Int J Hydrogen Energy 2020;45:27145–59.
[55] Steele BCH. Oxygen transport and exchange in oxide ceramics. J Power Sources 1994;49:1–14.
[56] Kharton VV, Figueiredo FM, Navarro L, Naumovich EN, Kovalevsky AV, Yaremchenko AA, et al. Ceria-based materials for solid oxide fuel cells. J Mater Sci 2001;36:1105–17.
[57] Gross MD, Vohs JM, Gorte RJ. An examination of SOFC anode functional layers based on ceria in YSZ. J Electrochem Soc 2007;154:B694–9.
[58] Das A, Paranjpe SK, Joy PA, Date SK. Neutron depolarization and diffraction studies in cluster glass $La_{0.5}Sr_{0.5}CoO_3$. J Alloys Compd 2001;326:101–4.
[59] Millburn JE, Green MA, Neumann DA, Rosseinsky MJ. Evolution of the structure of the K_2NiF_4 phases $La_{2-x}Sr_xNiO_{4+\delta}$ with oxidation state: octahedral distortion and phase separation ($0.2 \leq x \leq 1.0$). J Solid State Chem 1999;145:401–20.
[60] Vecino-Mantilla S, Zignani SC, Vannier R-N, Aricò AS, Lo Faro M. Insights on a Ruddlesden-Popper phase as an active layer for a solid oxide fuel cell fed with dry biogas. Renew Energy 2022;192:784–92.
[61] Huang K, Feng M, Goodenough JB, Milliken C. Electrode performance test on single ceramic fuel cells using as electrolyte Sr- and Mg-doped $LaGaO_3$. J Electrochem Soc 1997;144:3620–4.
[62] Barbucci A, Viviani M, Carpanese P, Vladikova D, Stoynov Z. Impedance analysis of oxygen reduction in SOFC composite electrodes. Electrochim Acta 2006;51:1641–50.
[63] Vladikova DE, Stoynov ZB, Barbucci A, Viviani M, Carpanese P, Kilner JA, et al. Impedance studies of cathode/electrolyte behaviour in SOFC. Electrochim Acta 2008;53:7491–9.
[64] Barfod R, Mogensen M, Klemensø T, Hagen A, Liu YL, Vang Hendriksen P. Detailed characterization of anode-supported SOFCs by impedance spectroscopy. J Electrochem Soc 2007;154:B371–8.
[65] Lin Y, Zhan Z, Liu J, Barnett SA. Direct operation of solid oxide fuel cells with methane fuel. Solid State Ionics 2005;176:1827–35.
[66] Macdonald JR, Johnson WB. Fundamentals of impedance spectroscopy. Impedance spectroscopy. John Wiley & Sons, Inc.; 2005. p. 1–26.